Published in final edited form as:
Acta Biomater. 2015 February ; 13: 168–176. doi:10.1016/j.actbio.2014.11.016.

Mild process to design silk scaffolds with reduced β-sheet structure and various topographies at nanometer scale

Yazhen Pei[a], **Xi Liu**[a], **Shanshan Liu**[a], **Qiang Lu**[a,*], **Jing Liu**[b], **David L Kaplan**[a,c], and **Hesun Zhu**[d]

[a]National Engineering Laboratory for Modern Silk & Collaborative Innovation C enterof Suzhou Nano Science and Technology, Soochow University, Suzhou 215123, People's Republic of China

[b]Regenerative Medicine Center, First Affiliated Hospital of Dalian Medical University, No.222 Zhongshan Road, Dalian 116011, People's Republic of China

[c]Department of Biomedical Engineering, Tufts University, Medford, MA 02155, USA

[d]Research Center of Materials Science, Beijing Institute of Technology, Beijing, 100081, People's Republic of China

Abstract

Three-dimensional (3D) porous silk scaffolds with good biocompatibility and minimal immunogenicity, have promising applications in different tissue regenerations. However, a challenge remains to effectively fabricate their microstructures and mechanical properties to satisfy specific requirements of different tissues. In this study, silk scaffolds were fabricated to form extracellular matrix (ECM) mimetic nanofibrous architecture in a mild process. A slowly increasing concentration process was applied to regulate silk self-assembly into nanofibers in aqueous solution. Then glycerol was blended with the nanofiber solution and induced silk crystallization in lyophilization process, endowing freeze-dried scaffolds water-stability. The glycerol was leached from the scaffolds, leaving similar porous structure at a micrometer scale but different topographies at nanoscale. Compared to previous salt-leached and methanol annealed scaffolds, the present scaffolds showed lower β-sheet content, softer mechanical property, and improved cell growth and differentiation behaviors, implying their promising future as platforms for controlling stem cell fate and soft tissue regeneration.

Keywords

Silk; ECM-mimic; Reduced β-sheet Structure; Soft Tissue

Corresponding author: Qiang Lu, Tel: (+86)-512-67061649; Lvqiang78@suda.edu.cn.

1. Introduction

Silk is a promising biomaterial for tissue engineering because of its biocompatibility, unique mechanical properties, ease of chemical modification, and biodegradability [1–6]. Recent studies have revealed the feasibility of silk as a supporting matrix for cells, including fibroblasts, osteoblasts, hepatocytes, nerve and stem cells, as well as a scaffolding for tissue engineering of bone, ligaments, blood vessels, skin, cartilage and other tissues [7–11]. Following the increasing applications, there remains a demand to further improve the bioactivity of silk scaffolds. Recent studies are now clarifying the significant influence of biomimetic nanostructures of biomaterials on cell behaviors [12], including better cell attachment and proliferation [6,13–18]. Electrospinning, an effective way to prepare biomimetic nanofibrous structures, was used to generate 2D and 3D silk constructs, such as sheets, tubes, and stacked sheets [19–23], but failed to generate 3-D scaffolds with microporous structures (pore size >100μm) and high thickness suitable for bone, cartilage, liver or muscle regenerations [24,25]. Other processing options, including salt leaching, gas foaming, and freeze-drying treatments [26–29], have achieved complex 3-D porous structure fabrications with tailored topography at micrometer scale, but still remained impracticable to regulate topographical properties at nanoscale [17,30–33].

Recently, nanofibrous silk scaffold with 3-D porous structure and better biocompatibility was successfully prepared by a modified lyophilization method in our laboratory [34,35]. Silk nanofiber solution was firstly prepared via a slowly increasing concentration process [36,37]. Then, scaffolds with porous structure instead of separate lamellar sheets were directly derived from the nanofiber solution after freeze-drying process [34]. However, methanol or water annealing treatments were required to achieve water insolubility, in which methanol was harmful for environment while water annealing partly sacrificed the porous structure [36]. A stiffness mismatch still existed between the formed scaffolds and soft tissues such as skin and muscle. Lu et al. once prepared insoluble silk films with glycerol as a plasticizer where glycerol regulated protein crystallization to achieve water-stability and tunable mechanical properties without after-treatments [38]. Unfortunately, glycerol is never used to generate insoluble silk scaffolds partly due to a failure of porous structure formation.

Based on previous studies, the present study addresses two goals. Firstly, we desired to design and prepare water-insoluble silk scaffolds with satisfactory microporous structure and nano-topography, improved biocompatibility, and tailored softer mechanical properties to improve their applicability in tissue engineering. Secondly, an all-aqueous process was preferentially applied to avoid the use of organic solvents. To achieve the objectives, glycerol was blended with silk nanofiber solution. Silk scaffolds with good microstructures and tunable mechanical properties were obtained by varying the glycerol content. Biocompatibility was evaluated by co-culture with rat bone marrow stem cells (rBMSCs).

2. Materials and Methods

2.1. Preparation of concentrated silk solution

B. mori silk solutions were prepared according to our previous published procedures [39]. Cocoons were boiled for 20 min in an aqueous solution of 0.02 M Na_2CO_3 and then rinsed

thoroughly with distilled water to extract the sericin proteins. After drying the extracted silk was dissolved in 9.3M LiBr solution at 60°C for 4 h, yielding a 20% (w/v) solution. This solution was dialyzed against distilled water using dialysis tube (MWCO 3500) for 72 h to remove the salt. Then the solution was centrifuged at 9000 r/min for 20 min at 4°C to remove silk aggregations formed during the process. The final concentration of silk in water was about 7 wt%, determined by weighing the remaining solid after drying. The fresh solution was concentrated at 60°C for 24 h in an oven, then further concentrated in laminar flow hood with airflow at 0.3m/s for 3 days to form concentrated silk solution (25–30 wt.%). Silk nanoparticles transformed into nanofibers in the concentration process (Figure S1). The fresh solution (silk nanoparticles) and concentrated solution (silk nanofibers) were then diluted to 2 wt% for subsequent lyophilized scaffold preparation.

2.2. Preparation of silk porous Scaffolds

Silk porous scaffolds were prepared according to a modified lyophilization method. Glycerol, an inductive agent for silk crystallization in film forming process [38], is applied to scaffold fabrication in our study. Although glycerol is still effective in inducing silk crystallization in lyophilization process (Figure S2), glycerol-treated scaffolds derived from fresh silk solution presented separate lamellar morphology (Figure S2) which limited their application in tissue engineering. Therefore silk nanofibers formed in a slowly increasing concentration process were blended with glycerol to restrain lamina formation and finally achieve water-insoluble silk scaffolds with microporous structure [36]. Simply, the diluted silk nanofiber solution was mixed with glycerol at silk/glycerol weight ratios of 80: 20, 70: 30, and 60: 40, respectively. The mixed solution was poured into a cylindrically shaped container, frozen at −20°C for 12 h, and then lyophilized for 48 h. After lyophilization, the dried scaffolds were rinsed in distilled water for above 48 h to remove glycerol [38]. Then the scaffolds were freeze-dried again for subsequent characterization. As a control, silk scaffolds derived from pure nanofiber solution were also prepared via the same lyophilization process and then stabilized with methanol treatment.

2.3. Characterization of Silk Fibroin/Glycerol Scaffolds

2.3.1. Scanning Electron Microscopy (SEM)—Silk scaffolds were fractured in liquid nitrogen and sputtered with gold. The morphologies of cross section of different scaffolds were imaged using SEM (S-4800, Hitachi, Tokyo, Japan) at 3 kV.

2.3.2. Atomic Force Microscope (AFM)—The morphology of silk in aqueous solution was observed by AFM (Veeco, Nanoscope V, Plain view, NY, America) in air. A 225 μm long silicon cantilever with a spring constant of 3 Nm^{-1} was used in tapping mode at 1.5 Hz scan rate. To prepare the samples for AFM imaging, different silk solutions were diluted to below 0.0001 wt% with deionized water [37]. Once diluted, 2 μl of the diluted silk solution was quickly dropped onto freshly cleaved 4×4 mm^2 mica surfaces and dried under a nitrogen gas.

2.3.3. Fourier Transform Infrared Spectroscopy (FTIR)—FTIR analysis of silk scaffolds was performed with a NICOLET FTIR 5700 spectrometer (Thermo Scientific, FL, U.S.A.), equipped with a MIRacle™ attenuated total reflection (Ge crystal). For each

measurement, 64 scans were co-added with a resolution of 4 cm^{-1}. The wavenumber ranged from 400 to 4000 cm^{-1}. Fourier self-deconvolution (FSD) of the infrared spectra covering the amide I region (1595–1705 cm^{-1}) was performed using Peakfit software to identify silk secondary structures [40].

2.3.4. X-ray Diffraction (XRD)—The crystalline of the obtained scaffolds was measured with X-ray diffraction (X' Pert-Pro MPD, PANalytical BV, Almelo, Holland) using monochromated Cu Kα radiation (30 mA, 40kV) with a scanning speed of 6°/min, and the 2θ range was from 5° to 45°.

2.3.5. Differential Scanning Calorimeter (DSC)—The thermal properties of the scaffolds were measured in a Q600 TGA/DSC instrument (TA Company, New Castle, DE) with purged dry nitrogen gas flow (50 mL/min). The instrument was calibrated with indium for heat flow and temperature. Aluminum and sapphire reference standards were used for calibration of the heat capacity. Standard mode DSC measurements were performed at a heating rate of 10°C/min.

2.3.6. Water solubility and Enzyme Degradation—Silk scaffolds (11 mm in diameter and 6 mm in height) were immersed in Milli-Q water in 50 mL tubes at scaffold/water weight ratio of 1: 99. The samples were kept at 37°C for 0.5 h, 2h, 4h, 8h, 12h, and 24h. The scaffolds were removed from water after incubation at each time point, and then dried in air at 60°C and weighed. The residual mass (%) was obtained by dividing residual weight by the initial weight. Five samples were carried out for each measurement.

The scaffolds were cultured in protease XIV solution (5 U ml^{-1} in PBS) to evaluate their degradation behaviors. Samples were soaked in protease XIV solution at scaffold/solution weight ratio of 1: 99 and then were kept at 37°C in a shaking water bath for 0.5h, 2h, 4h, 8h, 12h, 24h, 2d, 3d, 4d, 5d, 6d and 7d. At designated time points, five samples for each group were dried and weighed. The residual mass (%) was obtained by dividing residual weight by the initial weight.

2.3.7. Mechanical Properties—To measure the compressive properties of the scaffolds (11 mm in diameter and 22 mm in height) in wet conditions, the scaffolds were first hydrated in water for 4 h and then measured with a cross head speed of 2 mm/min at 25°C using an Instron 3365 testing frame (Instron, Norwood, MA) with a 500 N loading cell. The load was applied until the cylinder was compressed by more than 30% of its original length. The compressive modulus was calculated as the slope of the linear-elastic region of the stress-strain curve between 3% and 8% since the test was considered to begin once after the threshold stress (0.16 kPa) was reached[8]. Five samples were carried out for each group.

2.3.8. *In vitro* Biocompatibility of the Silk Scaffolds—Bone marrow mesenchymal stem cells (BMSCs) derived from SD rats were used to evaluate the *in vitro* biocompatibility of the scaffolds. The scaffolds were punched into small disks (with diameter of 8 mm and height of 2 mm) for 96-well plate, and sterilized with ^{60}Co γ-irradiation at the dose of 50 kGy. BMSCs were cultured in Dulbecco's modified Eagle medium (DMEM, low glucose) supplemented with 10% fetal bovine serum (FBS), 1% IU ml^{-1} streptomycin-penicillin (all

from Invitrogen, Carlsbad, CA). After reaching 90% confluence, cells were detached from Petri dish and seeded into the scaffolds at a density of 1.0×10^5 cell per well.

The cell morphology on the scaffolds was examined by confocal microscopy. After culture for 1 d, 6 d, and 12 d, the cell-seeded scaffolds were washed three times with PBS and fixed in 4% paraformaldehyde (Sigma-Aldrich, St Louis, MO) for 30 min, followed by further washing. The cells were permeabilized with 0.1% Triton X-100 for 5 min and incubated with FITC-phalloidin (Sigma-Aldrich, St. Louis, MO) for 20 min at room temperature, followed by washing with PBS and, finally, staining with DAPI (Sigma-Aldrich, St. Louis, MO) for 1 min. Representative fluorescence images of the stained samples were obtained using a confocal microscope (Olympus FV10 inverted microscope, Nagano, Japan) with excitation/emission at 358/462 nm and 494/518 nm. The images of the scaffolds were captured from the surface to a depth of 100 μm in increments of 10 μm. The cell morphology on the scaffolds was confirmed by SEM. After harvest the cell-seeded scaffolds were washed three times with PBS, fixed in 4% paraformaldehyde at room temperature, and then again washed three times with PBS. Fixed samples were dehydrated through a gradient of alcohol (50%, 70%, 80%, 90%, 100%, 100%) followed by lyophilization. After coated with gold, the samples were examined with SEM at the voltage of 10 kV. Several different areas of the specimens were randomly examined using a Hitachi model S-4800 scanning electron microscopy (Hitachi, Tokyo, Japan). Representative images are presented.

To study cell proliferation on the scaffolds, samples harvested at the indicated time points (from 1 to 12 d) were digested with proteinase K buffer solution for 16 h at 56°C, as described previously [18]. The DNA content was determined using the PicoGreen™ DNA assay, following the protocol of the manufacturer (Invitrogen, Carlsbad, CA). Samples (n=5) were measured at an excitation wavelength of 480 nm and emission wavelength of 530 nm, using a BioTeK Synergy 4 spectrofluorometer (BioTeK, Winooski, VT). The amount of DNA was calculated by interpolation from a standard curve prepared with λ-phage DNA in 10×10^{-3} M Tris-HCl (pH 7.4), 5×10^{-3} M NaCl, 0.1×10^{-3} M EDTA over a range of concentrations.

Myogenic gene expression and endothelial gene expression was investigated to assess cell differentiation on the scaffolds. At 1, 14 and 28 d, the total cellular RNA on the scaffolds was extracted with TRIZOL reagent (Invitrogen, Carlsbad, USA) and then analyzed through measuring the optical density at 260 nm with a Nano Drop 2000 (Thermo Scientific, Waltham, MA). 1 μg of the extracted RNA was reverse-transcribed into cDNA using a High-Capacity cDNA Reverse Transcription kit (Applied Biosystems, Carlsbad, USA) in a 2720 thermal cycler (Applied Biosystems, Foster City, CA, USA). Real-time PCR was performed at 95 °C (20 s), 40 cycles at 95 °C (3 s) and then 60 °C (30 s) successively with the Fast SYBR Green kit (Applied Biosystems, Carlsbad, USA) in a 7500 Real-Time PCR System (Applied Biosystems, Foster City, CA, USA). The relative expression levels determined with the delta Ct method were normalized against the Ct value of the reference gene GAPDH and further calibrated through the data of the methanol-treated scaffolds. Genes and primers are illustrated in Table 1. Each sample was measured in triplicate.

2.3.9 Statistical methods—All statistical analyses were performed using SPSS v.16.0 software. Comparison of the mean values of the data sets was performed using one-way AVOVA followed by the Student-Newman-Keuls test (SNK q-test). Measures are presented as means ± standard deviation, unless otherwise specified. $P < 0.05$ was considered significant.

3. Results and Discussion

3.1. Morphology of silk scaffolds

Figure 1 showed the microstructure and topography of the silk scaffolds regulated by different contents of glycerol. Different to laminar structure of silk scaffolds prepared with fresh solution (Fig S2), all silk scaffolds derived from the nanofiber solution with and without glycerol exhibited microporous structures (Figure 1 and Figure S3). The results confirmed the critical effect of silk nanofiber on porous structure formation in lyophilization process [36]. Different topographies at nanoscale appeared where globular nanostructures became more obvious on the pore surface following the glycerol increase in the scaffolds (Figure 1 A, C, E). The nanogranules with diameters greater than or similar to silk nanofibers should be part or aggregation of silk nanofibers, which has been observed in the glycerol-treated silk films [38]. After glycerol was leached out with water, nanofiber and nanopores with different sizes appeared on the surface of the pore wall without significant change of the porous structure (Figure 1 B, D, F). The nanofibrous structure became more obvious following the degradation process (Figure S4), confirming that the nanogranules before glycerol removal were derived from the nanofibers. Previous studies have suggested the impact of topographical cues such as nanofibers, nanopores, and nanocolumns on cellular performance [41–44]. The ECM-mimetic nanofibrous structure was considered to be favorable for cell growth [41–44]. Therefore silk scaffolds with similar microporous structure but different nano-topographies might have different influences on cell behaviors and facilitate cell proliferation following the nanofiber formation. On the other hand, compared to previous electrospun silk sheets, smaller-diameter nanofibers were achieved in our present study, which could supply larger surface area for cell adhesion and growth [13,16].

3.2. Structure analysis

Glycerol was blended with silk nanofiber solution to prepare water-insoluble scaffolds directly in our present work. Secondary structure changes of the silk scaffolds with glycerol treatment were determined with FTIR (Figure 2A). FSD of the infrared spectra in amide I (1595–1705 cm^{-1}) region was used to assess the contents of different secondary structures (Table 2). Based on previous studies [40,45], the secondary structures of silk include silk II, silk I, random structure, α-helix, and turns/bends where α-helix and turns/bends are intermediate states before silk I and silk II formation. Scaffold without glycerol (Figure 2Aa') maintained amorphous state in which the content of random coil was 38.5% (Table 2). Following the raise of glycerol content, silk I and silk II slightly increased while random coil and α-helix structure decreased in the silk scaffolds (Figure 2A and Table 2, b'–d'). The results indicated that glycerol could facilitate crystal structure formation in silk scaffolds, similar to that happened in silk film forming process [38]. After the removal of glycerol,

random coil was partly transformed to β-sheet structure (silk II) because of the release of structure restriction [38,46]. Interestingly, compared to methanol-treated scaffold, the glycerol-treated scaffolds had significantly lower and tunable β-sheet contents simply through changing glycerol contents. Although the adjustment extent is limited, the mechanical properties similar to different tissues could be achieved (Figure 4), making the scaffolds more suitable for different tissue regenerations.

Further study of the crystalline changes was carried out with XRD. Pure silk scaffolds showed an amorphous state, characterized by the broad featureless peak in XRD spanning from 12° to 32° (Figure 2Ba'). Then specific silk I peaks at 12.2° and 19.7° appeared for silk scaffolds with 20% glycerol (Figure 2Bb') [30]. Following further increase of glycerol in silk scaffolds, the peak at 20.7° became predominant, implying silk II formation (Figure 2Bc', d'). Silk I and silk II structures slightly changed in XRD spectra after the remove of glycerol. The results confirmed the regulation impact of glycerol on silk crystal structures. Compared to methanol-treated scaffolds, lower silk II peak intensity (20.7°) appeared in all the glycerol-treated scaffolds, in good agreement with the FTIR data.

Figure 2C illustrated standard DSC curves of the glycerol-treated silk scaffolds. Pure silk scaffold showed a significant bound water evaporation peak at 80°C, a small nonisothermal crystallization peak at 215°, and a clear degradation peak at 280°C (Figure 2Ca'). In comparison, the glycerol-treated scaffolds showed a small endothermic peak at above 170°C due to the glass transition (Tg) (Figure 2Cb'–d'), indicating higher crystallinity and thermal stability of the scaffolds. In addition, the bound water evaporation peaks disappeared in the curves of the glycerol-treated silk scaffolds since glycerol could replace water in silk chain hydration [38]. The crystallization peaks also disappeared, due to stable silk I and silk II formation. All the glycerol-treated scaffolds had higher degradation temperature than pure silk scaffold, but lower than methanol treated scaffold, which was consistent with FTIR and XRD results.

3.3. Water Solubility and Enzyme Degradation

The insolubility of silk scaffolds was determined by the weight loss of the scaffolds in water (Figure 3A). After the removal of glycerol, all the glycerol-treated silk scaffolds kept stable after a trace of weight loss at first 0.5 h while pure silk scaffold completely dissolved in water. Water stability of the scaffolds slightly increased with the increase of glycerol content without statistical significance. The results indicated that both silk I and silk II structures induced by glycerol endowed silk scaffolds water-stability. Then the *in vitro* enzyme degradation was carried out in protease XIV solution (Figure 3B). When the glycerol content increased in the scaffold forming process, the degradation rates of the formed scaffolds gradually decreased partly because of more silk II formation. All glycerol-treated silk scaffolds expressed higher degradation rate than methanol-treated scaffolds, implying the achievement of quicker and tunable degradation properties. To further understand the enzymatic degradation process, cross section morphology and structure composition of the scaffolds were studied with SEM (Figure S4), and FTIR (Figure S5), respectively. In enzymatic degradation process, silk I peaks disappeared gradually while silk II peaks became predominant for all the glycerol-treated scaffolds, suggesting slower degradation

rate of silk II than silk I. All these results implied that silk scaffolds with controlled degradation behavior were successfully prepared by glycerol-treated lyophilization process [47].

3.4. Mechanical property

Figure 4 showed the mechanical properties of the glycerol-treated silk scaffolds. Compressive modulus of the silk scaffolds treated by 20%, 30%, and 40% glycerol was about 15 kPa, 11 kPa and 6 kPa, respectively, significantly lower than that of methanol-treated scaffolds (30 kPa). Although having higher β-sheet content, the scaffolds treated by higher levels of glycerol became compliant probably because increased nanopores (Fig 1 B, D, F) reduced their stiffness. Many studies have revealed the influence of matrix elasticity on the differentiation of human mesenchymal stem cells [48–50]. Soft matrices with elastic modulus of 8–17 kPa could favor differentiation of BMSC into muscle cells while the matrices with elastic modulus of 1–7 kPa facilitate differentiation of BMSC into endothelial cells [51,52]. Therefore, the tailored mechanical properties of the scaffolds implied their promising future in different soft tissue regenerations.

3.5. *In vitro* Biocompatibility

rBMSCs attachment and proliferation were used to evaluate cell response on the scaffolds. Salt-leached silk scaffolds, prepared with fresh silk solution [53], were used as control to assess the influence of nanofibrous structure on cell behaviors. Figure 5 and 6 showed the typical cell attachment and growth behaviors on different silk scaffolds. Considering that the excellent cell-compatibility of silk-based scaffolds generally results in over-rapid growth of cells [54–56], lower initial cell seeding density was preferred, which resulted in lower cell growth within 6 days. Although the rBMSCs grew well on all the scaffolds from day 1 to day 12, cells formed continuous monolayer on the silk nanofiber-based scaffolds while distributed sparsely on salt-leached scaffolds at day 12 (Figure 6C), indicating the favorable action of nanofiber in cell proliferation. DNA results confirmed the cytocompatibility improvement of the nanofiber-based scaffolds (Figure 7). It has been well recognized that nanofibrous structure of ECM is a critical factor in regulating cell function. Silk nanofibers were firstly assembled in aqueous solution before lyophilization and then exposed to the cells following the scaffold dissolution and degradation (Figure 1 and Figure S4), offering more suitable microenvironment for cell proliferation [12].

The nanofiber-based scaffolds also showed different biocompatibility. Cell grew significantly better on the glycerol-treated scaffolds than on methanol-treated scaffolds (Figure 6 and 7). Previous study revealed that silk with reduced β-sheet structure could support cell adhesion and growth in an improved fashion [57], so it seems reasonable to consider lower β-sheet content of the glycerol-treated scaffolds as possible reason for the improvement. However, better cytocompatibility was found following the increase of β-sheet contents in the glycerol-treated silk scaffolds (Figure 6 and 7), contrary to the expectation. Considering that the increased glycerol not only resulted in β-sheet formation but also led to more nanopore and nanofiber exposure, the change of surface topography might be other factor in affecting the biocompatibility of silk scaffolds that has been confirmed in silk and other biomaterials [58–64]. The rougher nanostructure feature might

also further improve the biocompatibility of the glycerol-treated silk scaffolds compared to the methanol-treated scaffold (Figure S3). Although further studies are necessary to clarify the relation between biocompatibility and structure of silk scaffolds, our present results have indicated that biomimetic silk scaffolds with reduced β-sheet structures and better biocompatibility could be directly prepared through an all-aqueous process.

Compelling evidence has revealed the regulating action of biomaterial stiffness on stem cell differentiation [48–52]. Our present study would provide better matrices with stiffness that better matched with soft tissues such as muscle (E~10 kPa) and in vivo intima basement membrane (E~3kPa) [48,52,65]. A preliminary study was performed to reveal the influence of the scaffold stiffness on stem cell differentiation. The myogenic differentiation of rBMSCs was assessed by RT-qPCR of MyoD1 mRNA expression while the endothelial differentiation was evaluated by RT-qPCR of endothelial cell markers [66, 67]. Compared to that on methanol treated scaffolds, more rBMSCs differentiated into muscle cells on the 20% and 30% glycerol-treated silk scaffolds while higher amount of endothelial cells appeared on the 40% glycerol-treated silk scaffolds (Fig 8). The stem cell differentiation behaviors were coincident with the stiffness of the different scaffolds, suggesting that our scaffolds would be better candidates for soft tissue regenerations such as muscle.

4. Conclusions

Silk scaffolds with different nano-topographies were achieved to mimic the natural nanostructure of ECM by blending glycerol in an all-aqueous process. The secondary structures could be tailored by the content of glycerol, which in turn could control mechanical properties and degradation behaviors of the scaffolds. Considering the satisfactory biocompatibility and tunable mechanical properties, the silk scaffolds would be promising platform for the study of interaction between stem cell fate and biomaterials, and offer valuable matrices for different soft tissue regenerations.

Supplementary Material

Refer to Web version on PubMed Central for supplementary material.

Acknowledgments

We thank National Basic Research Program of China (973 Program 2013CB934400, 2012CB22302), NSFC (21174097, 81272106, 81271412) and the NIH (R01 DE017207) for support of this work. We also thank the Priority Academic Program Development of Jiangsu Higher Education Institutions (PAPD), the Excellent Youth Foundation of Jiangsu Province (BK2012009), International S&T Cooperation Project of the Ministry of S&T of China (2010DFR30850) and the Key Natural Science Foundation of the Jiangsu Higher Education Institutions of China (11KGA430002) for support of this work.

References

1. Altman GH, Diaz F, Jakuba C, Calabro T, Horan RL, Chen J, et al. Silk-based biomaterials. Biomaterials. 2003; 24:401–416. [PubMed: 12423595]
2. Liu H, Fan H, Wang Y, Toh SL, Goh JC. The interaction between a combined knitted silk scaffold and microporous silk sponge with human mesenchymal stem cells for ligament tissue engineering. Biomaterials. 2008; 29:662–674. [PubMed: 17997479]

3. Marolt D, Augst A, Freed LE, Vepari C, Fajardo R, Patel N, et al. Bone and cartilage tissue constructs grown using human bone marrow stromal cells, silk scaffolds and rotating bioreactors. Biomaterials. 2006; 27:6138–6149. [PubMed: 16895736]
4. Vepari C, Kaplan DL. Silk as a biomaterial. Prog Polym Sci. 2007; 32:991–1007. [PubMed: 19543442]
5. Zhang Y, Fan W, Ma Z, Wu C, Fang W, Liu G, et al. The effects of pore architecture in silk fibroin scaffolds on the growth and differentiation of mesenchymal stem cells expressing BMP7. Acta Biomater. 2010; 6:3021–3028. [PubMed: 20188872]
6. Chen JL, Yin Z, Shen WL, Chen X, Heng BC, Zou XH, et al. Efficacy of hESC-MSCs in knitted silk-collagen scaffold for tendon tissue engineering and their roles. Biomaterials. 2010; 31:9438–9451. [PubMed: 20870282]
7. Ziv K, Nuhn H, Ben-Haim Y, Sasportas LS, Kempen PJ, Niedringhaus TP, et al. A tunable silk-alginate hydrogel scaffold for stem cell culture and transplantation. Biomaterials. 2014; 35:3736–3743. [PubMed: 24484675]
8. Stoppato M, Stevens HY, Carletti E, Migliaresi C, Motta A, Guldberg RE. Effects of silk fibroin fiber incorporation on mechanical properties, endothelial cell colonization and vascularization of PDLLA scaffolds. Biomaterials. 2013; 34:4573–4581. [PubMed: 23522374]
9. Zhang Q, Zhao Y, Yan S, Yang Y, Zhao H, Li M, et al. Preparation of uniaxial multichannel silk fibroin scaffolds for guiding primary neurons. Acta Biomater. 2012; 8:2628–2638. [PubMed: 22465574]
10. Correia C, Bhumiratana S, Yan LP, Oliveira AL, Gimble JM, Rockwood D, et al. Development of silk-based scaffolds for tissue engineering of bone from human adipose-derived stem cells. Acta Biomater. 2012; 8:2483–2492. [PubMed: 22421311]
11. Wray LS, Tsioris K, Gil ES, Omenetto FG, Kaplan DL. Microfabricated porous silk scaffolds for vascularizing engineered tissues. Adv Funct Mater. 2013; 23:3404–3412. [PubMed: 24058328]
12. Woo KM, Jun JH, Chen VJ, Seo J, Baek JH, Ryoo HM, et al. Nano-fibrous scaffolding promotes osteoblast differentiation and biomineralization. Biomaterials. 2007; 28:335–343. [PubMed: 16854461]
13. Wang Y, Bella E, Lee CS, Migliaresi C, Pelcastre L, Schwartz Z, et al. The synergistic effects of 3-D porous silk fibroin matrix scaffold properties and hydrodynamic environment in cartilage tissue regeneration. Biomaterials. 2010; 31:4672–4681. [PubMed: 20303584]
14. Uebersax L, Mattotti M, Papaloizos M, Merkle HP, Gander B, Meinel L. Silk fibroin matrices for the controlled release of nerve growth factor (NGF). Biomaterials. 2007; 28:4449–4460. [PubMed: 17643485]
15. Toh S, Teh T, Vallaya S, Goh J. Novel silk scaffolds for ligament tissue engineering applications. Key Eng Mater. 2006; 326:727–730.
16. Teh K, Goh C, Toh S. Advanced micro-nano fibrous silk scaffold system for tendon/ligament tissue engineering. J Biomech. 2007; 40:S119–S120.
17. Mandal BB, Kundu SC. Cell proliferation and migration in silk fibroin 3D scaffolds. Biomaterials. 2009; 30:2956–2965. [PubMed: 19249094]
18. Chao PHG, Yodmuang S, Wang X, Sun L, Kaplan DL, Vunjak-Novakovic G. Silk hydrogel for cartilage tissue engineering. J Biomed Mater Res B. 2010; 95:84–90.
19. Fan L, Wang H, Zhang K, He C, Cai Z, Mo X. Regenerated silk fibroin nanofibrous matrices treated with 75% ethanol vapor for tissue-engineering applications. J Biomater Sci Polym Ed. 2012; 23:497–508. [PubMed: 21294970]
20. Zhao Y, Zhao W, Yu S, Guo Y, Gu X, Yang Y. Biocompatibility evaluation of electrospun silk fibroin nanofibrous mats with primarily cultured rat hippocampal neurons. Biomed Mater Eng. 2013; 23:545–554. [PubMed: 24165556]
21. Sahoo S, Toh SL, Goh JC. A bFGF-releasing silk/PLGA-based biohybrid scaffold for ligament/tendon tissue engineering using mesenchymal progenitor cells. Biomaterials. 2010; 31:2990–2998. [PubMed: 20089300]
22. Liu H, Li X, Zhou G, Fan H, Fan Y. Electrospun sulfated silk fibroin nanofibrous scaffolds for vascular tissue engineering. Biomaterials. 2011; 32:3784–3793. [PubMed: 21376391]

23. Zhang X, Baughman CB, Kaplan DL. In vitro evaluation of electrospun silk fibroin scaffolds for vascular cell growth. Biomaterials. 2008; 29:2217–2227. [PubMed: 18279952]
24. Prabhakaran MP, Venugopal JR, Ramakrishna S. Mesenchymal stem cell differentiation to neuronal cells on electrospun nanofibrous substrates for nerve tissue engineering. Biomaterials. 2009; 30:4996–5003. [PubMed: 19539369]
25. Meinel AJ, Kubow KE, Klotzsch E, Garcia-Fuentes M, Smith ML, Vogel V, et al. Optimization strategies for electrospun silk fibroin tissue engineering scaffolds. Biomaterials. 2009; 30:3058–3067. [PubMed: 19233463]
26. Kim UJ, Park J, Joo Kim H, Wada M, Kaplan DL. Three-dimensional aqueous-derived biomaterial scaffolds from silk fibroin. Biomaterials. 2005; 26:2775–2785. [PubMed: 15585282]
27. Lv Q, Feng Q. Preparation of 3-D regenerated fibroin scaffolds with freeze drying method and freeze drying/foaming technique. J Mater Sci Mater Med. 2006; 17:1349–1356. [PubMed: 17143767]
28. Tamada Y. New process to form a silk fibroin porous 3-D structure. Biomacromolecules. 2005; 6:3100–3106. [PubMed: 16283733]
29. Nazarov R, Jin HJ, Kaplan DL. Porous 3-D scaffolds from regenerated silk fibroin. Biomacromolecules. 2004; 5:718–726. [PubMed: 15132652]
30. Bhardwaj N, Kundu SC. Chondrogenic differentiation of rat MSCs on porous scaffolds of silk fibroin/chitosan blends. Biomaterials. 2012; 33:2848–2857. [PubMed: 22261099]
31. Mandal BB, Kundu SC. Osteogenic and adipogenic differentiation of rat bone marrow cells on non-mulberry and mulberry silk gland fibroin 3D scaffolds. Biomaterials. 2009; 30:5019–5030. [PubMed: 19577292]
32. Mandal BB, Ghosh B, Kundu S. Non-mulberry silk sericin/poly (vinyl alcohol) hydrogel matrices for potential biotechnological applications. Int J Biol Macromol. 2011; 49:125–133. [PubMed: 21549749]
33. Bhardwaj N, Kundu SC. Silk fibroin protein and chitosan polyelectrolyte complex porous scaffolds for tissue engineering applications. Carbohyd Polym. 2011; 85:325–333.
34. Lin S, Lu G, Liu S, Bai S, Liu X, Lu Q, et al. Nanoscale control of silks for nanofibrous scaffold formation with an improved porous structure. J Mater Chem B. 2014; 2:2622–2633.
35. Liu S, Dong C, Lu G, Lu Q, Li Z, Kaplan DL, et al. Bilayered vascular grafts based on silk proteins. Acta Biomater. 2013; 9:8991–9003. [PubMed: 23851155]
36. Lu Q, Wang X, Lu S, Li M, Kaplan DL, Zhu H. Nanofibrous architecture of silk fibroin scaffolds prepared with a mild self-assembly process. Biomaterials. 2011; 32:1059–1067. [PubMed: 20970185]
37. Lu Q, Zhu H, Zhang C, Zhang F, Zhang B, Kaplan DL. Silk Self-Assembly Mechanisms and Control From Thermodynamics to Kinetics. Biomacromolecules. 2012; 13:826–832. [PubMed: 22320432]
38. Lu S, Wang X, Lu Q, Zhang X, Kluge JA, Uppal N, et al. Insoluble and flexible silk films containing glycerol. Biomacromolecules. 2010; 11:143–150. [PubMed: 19919091]
39. Han F, Liu S, Liu X, Pei Y, Bai S, Zhao H, et al. Woven silk fabric-reinforced silk nanofibrous scaffolds for regenerating load-bearing soft tissues. Acta Biomater. 2014; 10:921–930. [PubMed: 24090985]
40. Lu Q, Hu X, Wang X, Kluge JA, Lu S, Cebe P, et al. Water-insoluble silk films with silk I structure. Acta Biomater. 2010; 6:1380–1387. [PubMed: 19874919]
41. Pan HA, Hung YC, Sui YP, Huang GS. Topographic control of the growth and function of cardiomyoblast H9C2 cells using nanodot arrays. Biomaterials. 2012; 33:20–28. [PubMed: 21982297]
42. Beachley V, Wen X. Polymer nanofibrous structures: Fabrication, biofunctionalization, and cell interactions. Prog polym Sci. 2010; 35:868–892. [PubMed: 20582161]
43. Anselme K, Bigerelle M. Role of materials surface topography on mammalian cell response. Int Mater Rev. 2011; 56:243–266.
44. von der Mark K, Park J, Bauer S, Schmuki P. Nanoscale engineering of biomimetic surfaces: cues from the extracellular matrix. Cell Tissue Res. 2010; 339:131–153. [PubMed: 19898872]

45. Hu X, Kaplan D, Cebe P. Determining beta-sheet crystallinity in fibrous proteins by thermal analysis and infrared spectroscopy. Macromolecules. 2006; 39:6161–6170.
46. Hu X, Kaplan D, Cebe P. Dynamic protein-water relationships during β-sheet formation. Macromolecules. 2008; 41:3939–3948.
47. Wang Y, Rudym DD, Walsh A, Abrahamsen L, Kim HJ, Kim HS, et al. In vivo degradation of three-dimensional silk fibroin scaffolds. Biomaterials. 2008; 29:3415–3428. [PubMed: 18502501]
48. Engler AJ, Sen S, Sweeney HL, Discher DE. Matrix elasticity directs stem cell lineage specification. Cell. 2006; 126:677–689. [PubMed: 16923388]
49. Lapin MR, Gonzalez JM, Johnson SE. Substrate elasticity affects bovine satellite cell activation kinetics in vitro. J Anim Sci. 2013; 91:2083–2090. [PubMed: 23463548]
50. Leipzig ND, Shoichet MS. The effect of substrate stiffness on adult neural stem cell behavior. Biomaterials. 2009; 30:6867–6878. [PubMed: 19775749]
51. Mathur AB, Collinsworth AM, Reichert WM, Kraus WE, Truskey GA. Endothelial, cardiac muscle and skeletal muscle exhibit different viscous and elastic properties as determined by atomic force microscopy. J Biomech. 2001; 34:1545–1553. [PubMed: 11716856]
52. Wingate K, Bonani W, Tan Y, Bryant SJ, Tan W. Compressive elasticity of three-dimensional nanofiber matrix directs mesenchymal stem cell differentiation to vascular cells with endothelial or smooth muscle cell markers. Acta Biomater. 2012; 8:1440–1449. [PubMed: 22266031]
53. Yao D, Dong S, Lu Q, Hu X, Kaplan DL, Zhang B, et al. Salt-leached silk scaffolds with tunable mechanical properties. Biomacromolecules. 2012; 13:3723–3729. [PubMed: 23016499]
54. Kim HJ, Park SH, Durham J, Gimble JM, Kaplan DL, Dragoo JL. In vitro chondrogenic differentiation of human adipose-derived stem cells with silk scaffolds. J Tissue Eng. 2012; 3:1–8.
55. Thimm BW, Wüst S, Hofmann S, Hagenmüller H, Müller R. Initial cell pre-cultivation can maximize ECM mineralization by human mesenchymal stem cells on silk fibroin scaffolds. Acta Biomater. 2011; 7:2218–2228. [PubMed: 21300186]
56. Talukdar S, Nguyen QT, Chen AC, Sah RL, Kundu SC. Effect o f initial cell seeding density on 3D-engineered silk fibroin scaffolds for articular cartilage tissue engineering. Biomaterials. 2011; 32:8927–8937. [PubMed: 21906805]
57. Jin HJ, Park J, Karageorgiou V, Kim UJ, Valluzzi R, Cebe P, et al. Water-stable silk films with reduced β-sheet content. Adv Funct Mater. 2005; 15:1241–1247.
58. Stary V, Douderova M, Bacakova L. Influence of surface roughness of carbon materials on human osteoblast-like cell growth. J Biomed Mater Res A. 2013:1–12. 00A. [PubMed: 22566462]
59. Gittens RA, McLachlan T, Olivares-Navarrete R, Cai Y, Berner S, Tannenbaum R, et al. The effects of combined micron-/submicron-scale surface roughness and nanoscale features on cell proliferation and differentiation. Biomaterials. 2011; 32:3395–3403. [PubMed: 21310480]
60. Ranella A, Barberoglou M, Bakogianni S, Fotakis C, Stratakis E. Tuning cell adhesion by controlling the roughness and wettability of 3D micro/nano silicon structures. Acta Biomater. 2010; 6:2711–2720. [PubMed: 20080216]
61. Wirth C, Comte V, Lagneau C, Exbrayat P, Lissac M, Jaffrezic-Renault N, et al. Nitinol surface roughness modulates in vitro cell response: a comparison between fibroblasts and osteoblasts. Mat Sci Eng C. 2005; 25:51–60.
62. Ross AM, Jiang Z, Bastmeyer M, Lahann J. Physical aspects of cell culture substrates: topography, roughness, and elasticity. Small. 2012; 8:336–355. [PubMed: 22162324]
63. Aboushelib MN, Osman E, Jansen I, Everts V, Feilzer AJ. Influence of a nanoporous zirconia implant surface of on cell viability of human osteoblasts. J Prosthodont. 2013; 22:190–195. [PubMed: 23432766]
64. Hu X, Park SH, Gil ES, Xia XX, Weiss AS, Kaplan DL. The influence of elasticity and surface roughness on myogenic and osteogenic-differentiation of cells on silk-elastin biomaterials. Biomaterials. 2011; 32:8979–8989. [PubMed: 21872326]
65. Peloquin J, Huynh J, Williams RM, Reinhart-King CA. Indentation measurements of the subendothelial matrix in bovine carotid arteries. J Biomech. 2011; 44:815–821. [PubMed: 21288524]

66. Toma C, Pittenger MF, Cahill KS, Byrne BJ, Kessler PD. Human mesenchymal stem cells differentiate to a cardiomyocyte phenotype in the adult murine heart. Circulation. 2002; 105:93–98. [PubMed: 11772882]

67. Bardouille C, Lehmann J, Heimann P, Jockusch H. Growth and differentiation of permanent and secondary mouse myogenic cell lines on microcarriers. Appl Microbiol Biot. 2001; 55:556–562.

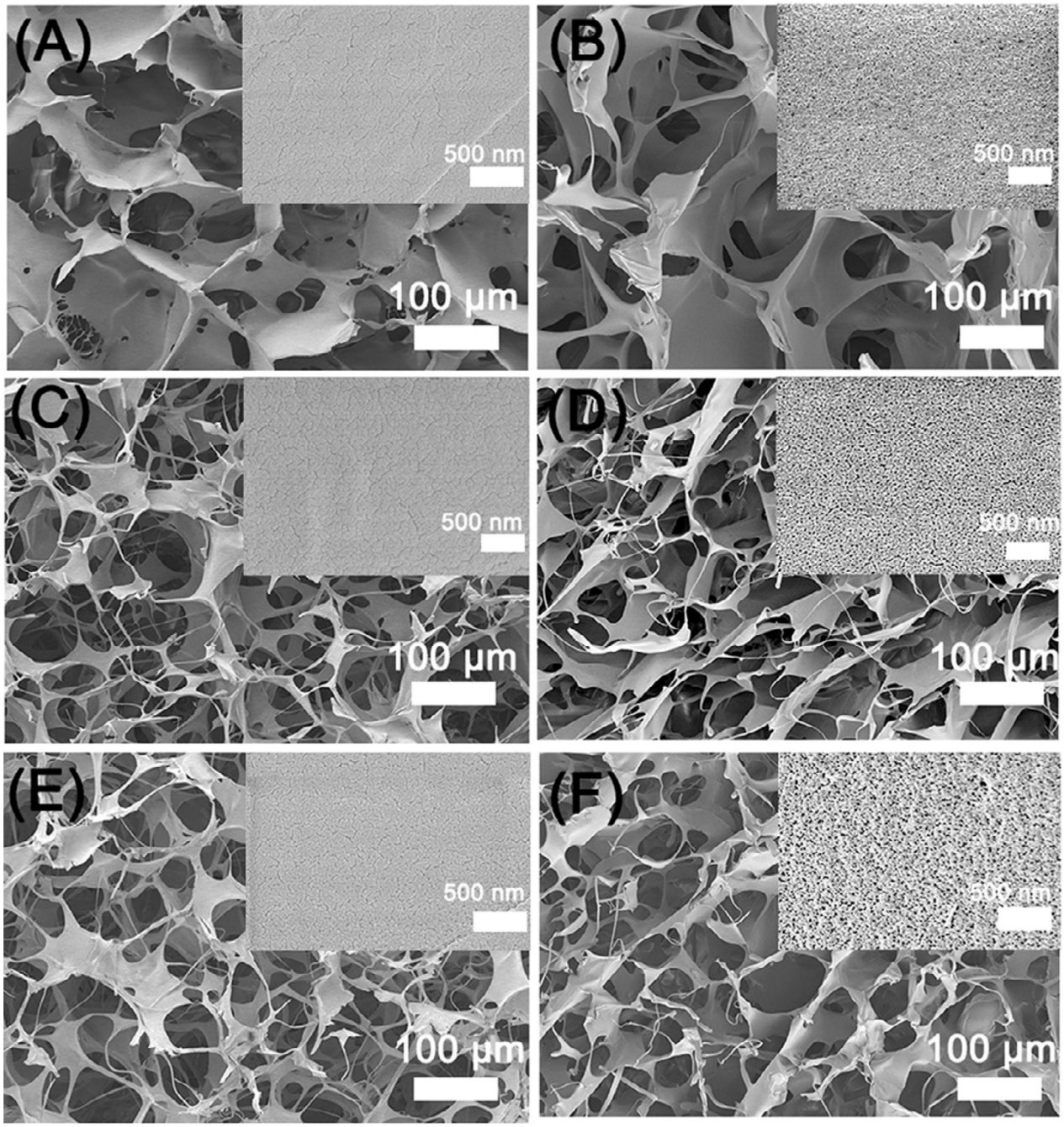

Figure 1.

SEM morphologies of glycerol-treated silk scaffolds before and after glycerol removal: The glycerol contents in silk scaffolds were 20% (A), 30% (C), and 40% (E), respectively. The corresponding scaffolds for A, C, and E after the glycerol removal were samples B, D and F. The inserted images showed the nanoscaled topography of pore wall with higher magnification.

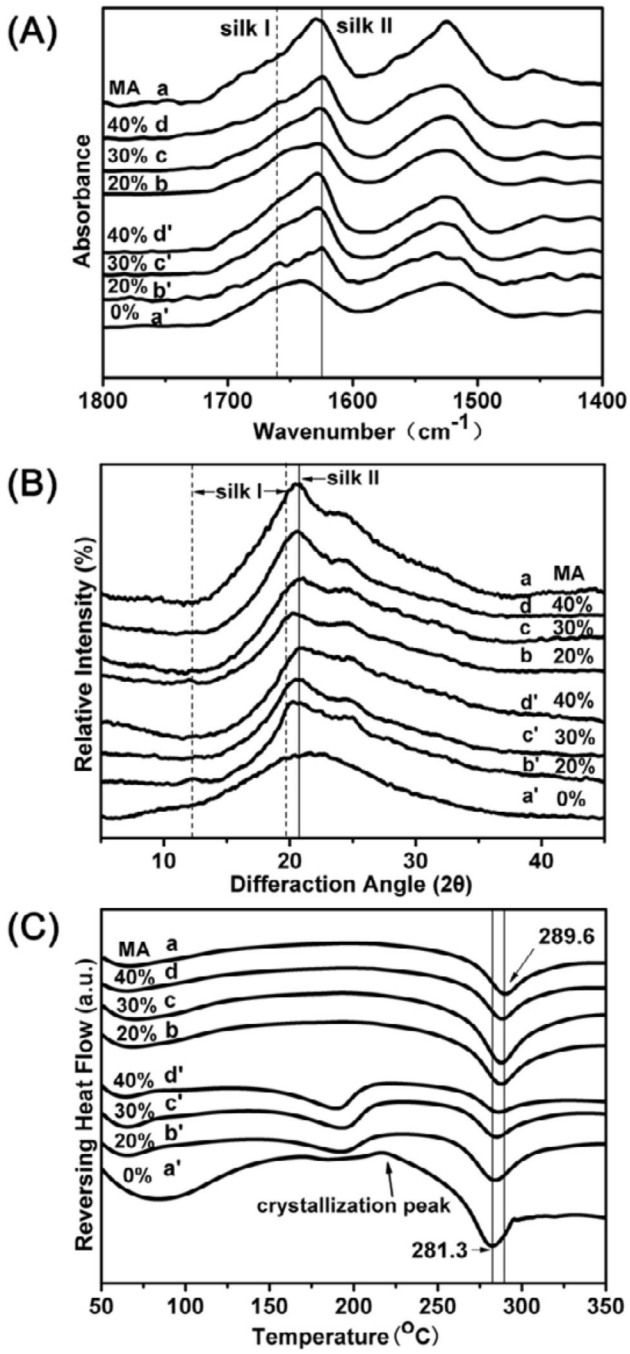

Figure 2.

FTIR, XRD, and DSC characterization of silk scaffolds with different glycerol contents: The glycerol contents for samples (a'), (b'), (c'), and (d') were 0%, 20%, 30% and 40%, respectively. Sample (a) is methanol-treated scaffold of (a'). The corresponding scaffolds for (b'), (c'), and (d') were samples (b), (c), and (d) after the removal of glycerol in water.

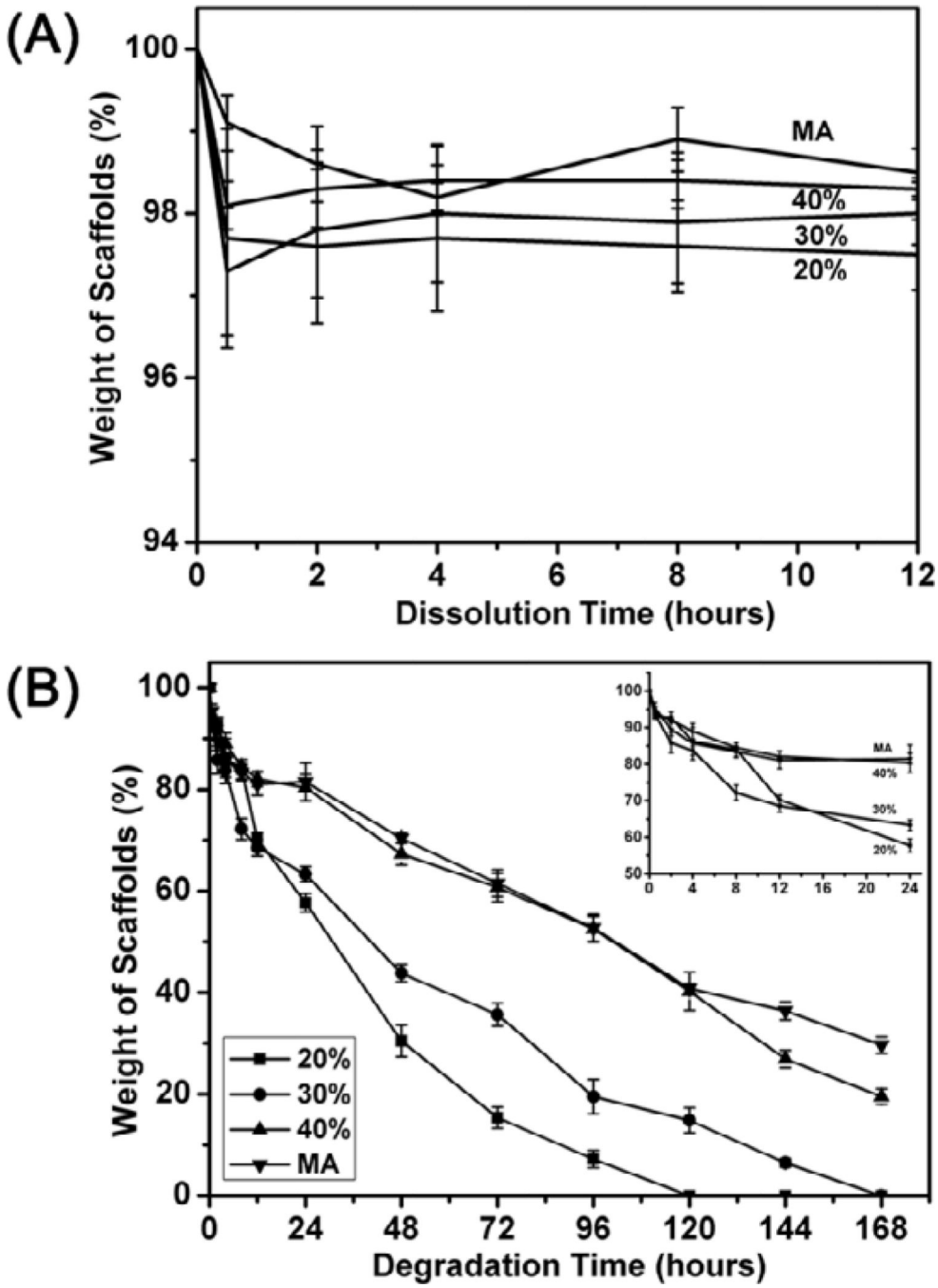

Figure 3.

Water solubility (A) and enzyme degradation (B) of the glycerol-treated silk scaffolds after the removal of glycerol in water: The percentages inside curves were the contents of glycerol before glycerol removal while MA indicated methanol-treated silk scaffolds without glycerol treatment. For water solubility, the samples were immersed in Milli-Q water in 50 mL tubes at scaffold/water weight ratio of 1: 99 at 37°C. In enzyme degradation process, the samples were cultured in protease XIV solution (5 U ml^{-1} in PBS) at 37°C.

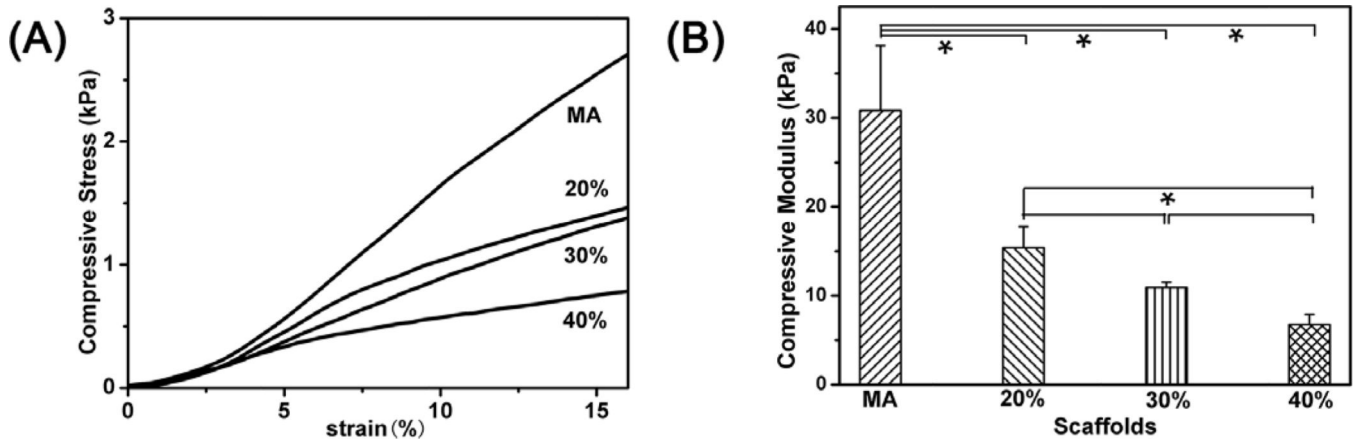

Figure 4.

Typical stress–strain curves and compressive modulus of the glycerol-treated silk scaffolds after the removal of glycerol in wet conditions. The compressive modulus was calculated as the slope of the linear-elastic region of the stress-strain curve between 3% and 8%. The percentages inside curves were the contents of glycerol before glycerol removal while MA indicated methanol-treated silk scaffolds without glycerol treatment.

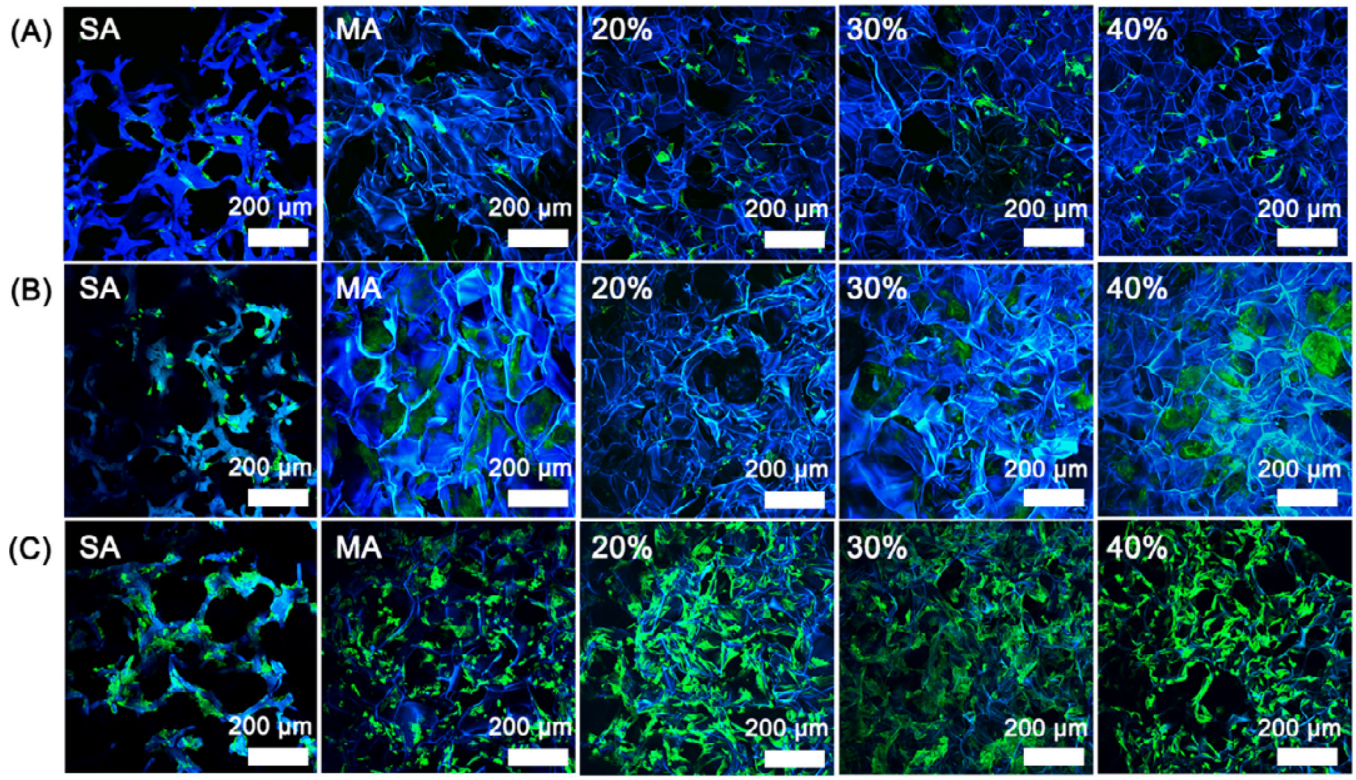

Figure 5.

Fluorescence microscopy images of rBMSC cultured on the glycerol-treated silk scaffolds after the removal of glycerol: (A) 1st day; (B) 6th day; (C) 12th day. The percentages inside images were the contents of glycerol before glycerol removal while SA and MA indicated salt-leached silk scaffolds and methanol-treated silk scaffolds without glycerol treatment. Blue (DAPI) for nuclei and silk fibroin scaffolds; green (FITC labeled phalloidin) for F-actin.

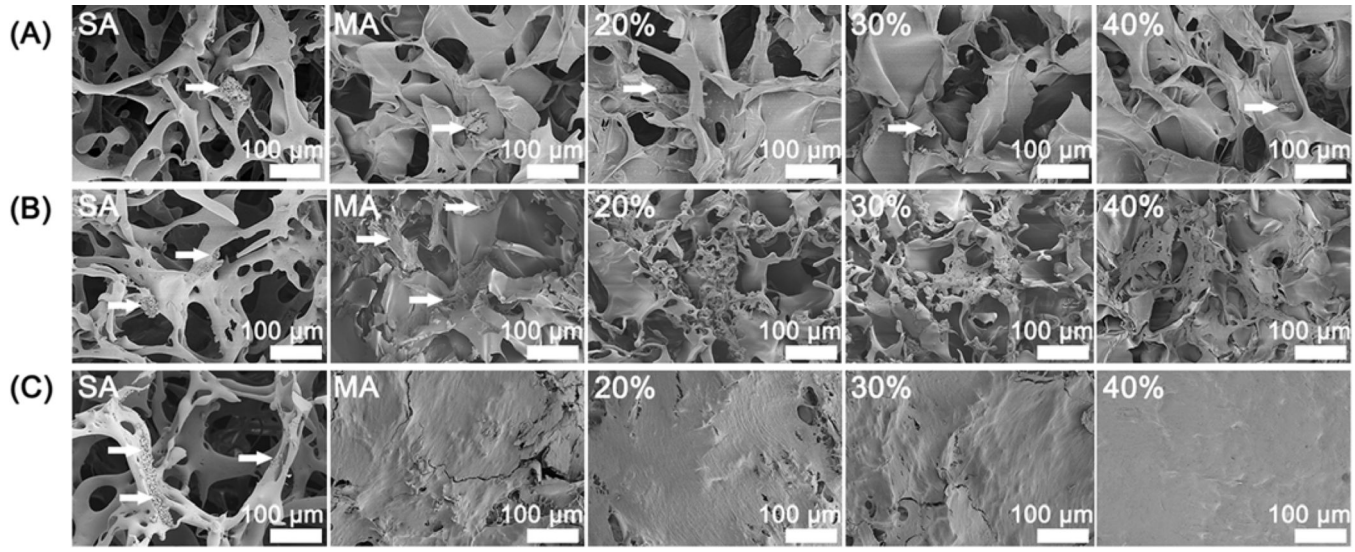

Figure 6.

SEM morphology of rBMSC cultured on the glycerol-treated silk scaffolds after the removal of glycerol: (A) 1st day; (B) 6th day; (C) 12th day. The percentages inside images were the contents of glycerol before glycerol removal while SA and MA indicated salt-leached silk scaffolds and methanol-treated silk scaffolds without glycerol treatment. The arrows were pointed to the cells on the scaffolds.

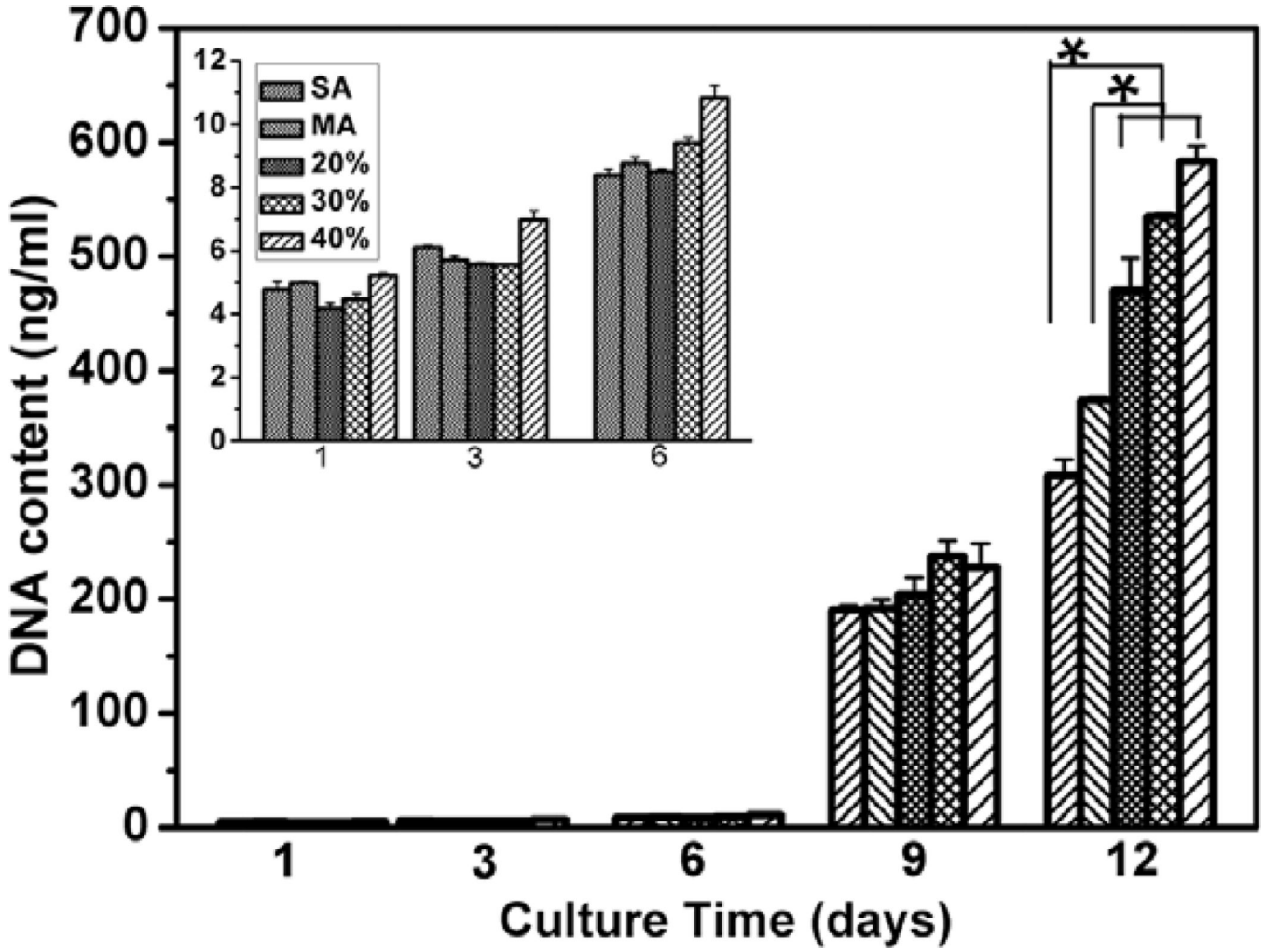

Figure 7.

rBMSC proliferation on different silk scaffolds measured with DNA analysis. The percentages were the contents of glycerol before glycerol removal while SA and MA indicated salt-leached silk scaffolds and methanol-treated silk scaffolds without glycerol treatment. Inset is the DNA content of the first 6 days. *statistically significant $P<0.05$.

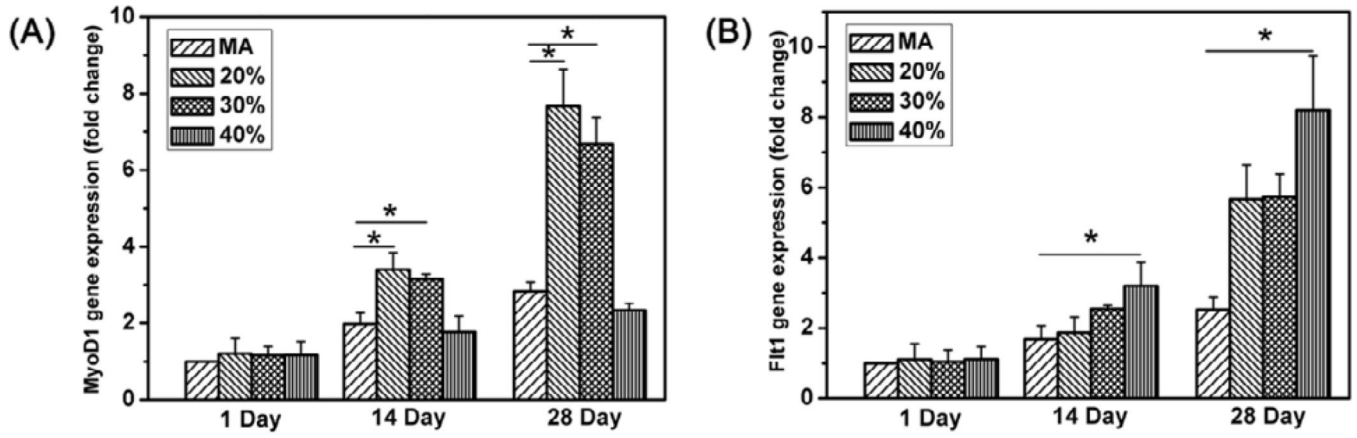

Figure 8.

mRNA levels of MyoD1(A) and Flt(B) on different scaffolds at day 1, day 14 and day 28 quantified by real-time PCR. Expression of MyoD1 and Flt is normalized to GAPDH. The percentages were the contents of glycerol before glycerol removal while MA indicated methanol-treated silk scaffolds without glycerol treatment.*statistically significant $P<0.05$.

Table 1

Sequences of primers used in real-time PCR (PR-PCR).

Genes	Primer Sequence (F, R, 5′-3′)	Product Length (bp)
GAPDH	TGGGTGTGAACCACGAGAA	143
	GGCATGGACTGTGGTCATGA	
MyoD1	TGGGACATGGAGCTACTATCGC	119
	GGTGAGTCGAAACACGGATCAT	
Flt-1	CGGAGAAATCTGCTCGCTAT	190
	CTTGGAAGGGACGACACG	

Table 2

FTIR determination of secondary structures of different silk scaffolds through Fourier self-deconvolution (FSD) of the amide I region.

	Secondary Structure Content (%)					
	Side chains 1590–1605 cm^{-1}	**Silk II, β-sheet 1610–1635 cm^{-1} 1695–1700 cm^{-1}**	**Random coil 1635–1645 cm^{-1}**	**Silk I, type II-turn 1647–1654 cm^{-1}**	**α-helix 1658–1664 cm^{-1}**	**Turns and bends 1666–1695 cm^{-1}**
a	0.87 ± 0.03	46.19 ± 1.24	15.34 ± 1.87	12.38 ± 1.12	5.33 ± 0.97	19.89 ± 0.51
b	0.87 ± 0.01	31.35 ± 2.16	15.77 ± 1.34	21.70 ± 0.64	6.83 ± 0.99	23.49 ± 0.31
c	0.55 ± 0.03	36.99 ± 1.26	13.83 ± 1.69	22.81 ± 1.24	4.85 ± 0.09	20.90 ± 1.15
d	0.64 ± 0.03	42.03 ± 1.97	11.90 ± 0.42	23.87 ± 0.63	2.76 ± 0.07	18.80 ± 1.29
a’	0.01 ± 0.01	23.20 ± 1.20	38.54 ± 2.33	9.01 ± 1.31	9.77 ± 1.62	20.90 ± 0.34
b’	0.76 ± 0.09	28.42 ± 1.34	18.61 ± 2.10	18.45 ± 1.65	7.87 ± 0.95	25.98 ± 0.04
c’	0.55 ± 0.02	31.39 ± 2.30	17.47 ± 0.14	20.52 ± 0.59	7.45 ± 1.36	22.62 ± 1.40
d’	0.76 ± 0.04	35.04 ± 1.29	12.61 ± 1.60	22.96 ± 2.06	5.24 ± 0.08	23.39 ± 0.98

a, Methanol-treated silk scaffolds without glycerol treatment;

b–d, silk scaffolds treated with 20%, 30%, and 40% glycerol, and after the removal of glycerol, respectively.

a’–d’, silk scaffolds treated with 0%, 20%, 30% and 40% glycerol but without the removal of glycerol, respectively.